Evaluation of Methods of Design for Strongback Braced Frames

Peter C. Talley, S.M.ASCE[1]; Mark D. Denavit, Ph.D., M.ASCE[2]; Nicholas. E. Wierschem, Ph.D., A.M.ASCE[3]

[1] Graduate Research Assistant, University of Tennessee, Knoxville.
[2] Associate Professor, University of Tennessee, Knoxville. Email: mdenavit@utk.edu
[3] Associate Professor, University of Tennessee, Knoxville.

ABSTRACT

Strongback braced frames (SBF) are a relatively new structural system intended to reduce structural damage during seismic events and improve resilience. SBFs combine buckling-restrained braces, which provide the primary lateral resistance and energy dissipation, with a stiff elastic spine to distribute demands across the height of the structure and prevent the formation of weak- and soft-story mechanisms. Designing the spine is challenging, as higher mode effects and partial yield mechanisms have been shown to be significant. These effects, and their interaction, are not fully accounted for by standardized design methods. It is also unclear how stiff and strong the spine must be in order to achieve the desired behaviors. There are proposed procedures for designing SBFs, however they have not been broadly evaluated and they have not been compared. This work evaluates two proposed design procedures, the simplified modal pushover analysis (SMPA) and generalized modified modal superposition (GMMS), with a "control" procedure based on current standardized capacity design procedures. A total of nine frames were designed for three buildings using the three procedures. Nonlinear response history analyses were performed to evaluate the differences in behavior resulting from the different design methods. To determine the effect of the strength and stiffness of the strongback, the yield strength and elastic modulus of the strongback members were varied and the analyses repeated. The results of this work show that the GMMS and SMPA design procedures are generally well-calibrated and provide benefit over current standardized procedures in several ways: collapse performance is improved, and yielding in the strongback and residual drifts are reduced. The GMMS procedure results in larger members, but provides similar outcomes to the more-complicated-to-implement SMPA. The insights from this work will assist engineers when implementing these design methods, and support the codification of strongback braced frames in design standards.

Keywords: strongback braced frame, elastic spine, nonlinear analysis, design

INTRODUCTION

Modern seismic design provisions focus on preventing collapse and ensuring the survival of the occupants of a structure during an earthquake. These minimum goals, however, do not ensure that structures are able to be used after a significant seismic event. As a result, the structure may not be useable for habitation or other vital services, and can require significant repairs or even complete demolition. More resilient structures, ones which have reduced risk of collapse and experience less structural damage, can reduce the downtime after a seismic event and reduce long-term costs associated with repair and refit (Bruneau and Reinhorn 2006).

Important structures, such as the hospitals and fire stations assigned to ASCE 7-22 Risk Category IV, can, in effect, be designed to be more resilient by increasing the design-level demands but otherwise following a design procedure based predominantly on collapse prevention (ASCE 2022). A more explicit evaluation of resilience can be made through performance-based design, such as the procedures available in ASCE 41-17 or Chapter 16 of ASCE 7-22 (ASCE 2017, 2022). Some seismic force resisting systems, that are specifically intended to reduce damage during an earthquake, can result in buildings that are intrinsically more resilient.

Spine systems are a class of seismic force resisting-systems intended to reduce overall structural damage during an earthquake by preventing the accrual of damage in a single story or set of stories. In these systems, an elastic spine runs the entire height of the structure, providing vertical continuity between all levels and energy-dissipating mechanisms. Examples of spine systems include steel rocking frames (Eatherton et al. 2014; Roke 2010), concrete rocking walls (Kurama et al. 1999; Priestley et al. 1978, 1999) and strongback braced frames (Lai and Mahin 2014; Simpson 2018; Tremblay 2003).

Strongback braced frames (SBF) are a variation on concentrically braced frames and buckling-restrained braced frames, using one half of the frame as the energy-dissipating component and the other half as the spine (here termed the strongback). An example SBF is shown in Fig. 1.

The most common energy-dissipating component proposed for SBFs are buckling-restrained braces (BRB), though other components such as conventional braces and viscous dampers have also been studied (Abolghasemi et al. 2024; Lai and Mahin 2014; Palermo et al. 2021). In this work, BRBs are used to provide both the primary lateral resistance and the primary energy dissipation capacity of the frame.

The spine in SBFs is configured as a steel truss, with tie braces to provide vertical continuity between levels in the spine. Under severe ground motions, the spine is intended to remain elastic and pivot about its base while the BRBs yield, imposing a first-mode deformation pattern (Lai and Mahin 2014). As the full yielding mechanism develops, demands are transferred between stories through the spine, allowing the BRBs at all levels to participate concurrently, and preventing runaway damage concentrations caused by the loss of stiffness due to yielding. The buckling-restrained braces and the spine are tightly integrated, allowing the BRBs at all levels to be fully engaged, with demands distributed vertically by the strongback. With a strong and stiff enough spine, SBFs allow full development of the BRB hysteresis and significant energy dissipation at every level, while preventing accumulation of damage in a single story.

The remaining beams and columns in the frame serve primarily to support gravity loads and complete the load path of the seismic force-resisting system. The beams also serve as a secondary source of energy dissipation, through plastic hinging at the face of the strongback. The opposing column is not expected to see significant inelastic demands. The connections throughout the frame are standard braced frame connections. Within the strongback itself, the connections are expected to experience less ductility demand than those in a conventional braced frame, due to the strongback remaining elastic.

Designing a strongback braced frame to achieve its intended behavior can be challenging. Current linear seismic design methods (ASCE 2022) and traditional capacity design (AISC 2016b) do not sufficiently account for the demands on the strongback. As the spine is intended to remain elastic and distribute demand after the buckling-restrained braces yield, (1) demands on the spine are not limited by yielding and (2) a significant proportion of the demand is associated with higher mode response (Gioiella et al. 2018; Simpson 2020). The higher mode response can be mitigated by modifications to the frame, such as by using multiple rocking or pivoting segments in the spine (Broujerdian and Mohammadi Dehcheshmeh 2022; Wiebe and

Christopoulos 2009). The beams are also subject to significant rotational demand at the face of the strongback. It has been suggested that the beam rotations at the face of the strongback be designed as displacement-controlled actions, thus incorporating them directly into the energy dissipation system by allowing them to yield, with their size limited either by explicitly evaluated displacement limits or implicitly through force reduction (Simpson and Mahin 2018).

While it is possible to evaluate the demands on the strongback using nonlinear dynamic analysis, this requires significant time, resources, and expertise, which may not be available to most design firms. Thus, it is strongly desirable to have a simpler method for determining demands on the spine. Several simplified methods have been proposed for the design of SBFs in specific and spine frames in general, varying from analytical estimations of the story shear and overturning moment (Wiebe and Christopoulos 2015) to more complicated modal analyses (Bosco et al. 2018; Martin and Deierlein 2021; Roke et al. 2009; Steele and Wiebe 2016), to nonlinear analysis of the frame (Simpson and Rivera Torres 2021). Investigated here are the simplified modal pushover analysis (SMPA) procedure (Simpson and Rivera Torres 2021) and the generalized modified modal superposition (GMMS) procedure (Martin and Deierlein 2021).

The SMPA procedure (Simpson and Rivera Torres 2021), developed as a simplification of modal pushover analysis (Chopra and Goel 2002), explicitly considers the plastic mechanism of the SBF. A displacement-controlled analysis is used in the first mode, and load-controlled analyses up to a per-mode base shear are used in the higher modes. There are several options for modeling of the plastic behavior, ranging from highly detailed asymmetric hysteretic response to neglecting nonlinear behavior entirely. Simpson and Rivera Torres (2021) recommend using elastic-perfectly-plastic materials for the BRBs in the first mode and elastic materials in the higher modes, with post-analysis checks to ensure that behavior remains within the design strength range.

The GMMS procedure (Martin and Deierlein 2021) is simpler than the SMPA procedure, as no inelastic analysis is performed. GMMS was developed as an extension of the modified modal superposition procedure (Martin et al. 2019; Priestley and Amaris 2003) to steel rocking and pivoting spine frames, and is similar to other modal response-spectrum based procedures (Roke et al. 2009; Steele and Wiebe 2016).

Unlike SMPA, GMMS does not provide information about the design of displacement-controlled components in the frame (i.e., the members and connections designed to experience inelasticity), and is instead solely used for the design of the spine and other force-controlled components (i.e., the members and connections expected to remain essentially elastic). It was developed and tested primarily on rocking frames and is less well-defined for strongback braced frames. The procedure uses an equivalent single-degree-of-freedom system to estimate the system stiffness at the maximum considered earthquake (MCE), and replaces the energy-dissipating elements with equivalent stiffness springs. These springs are sized to provide the same system overturning resistance at MCE, with stiffness kept proportional to the stiffness of the elements they are replacing.

Of these two approaches, it is unknown which provides the best required strengths for design. It also remains unclear precisely how stiff and strong the strongback must be to enforce the desired behavior. Neither the SMPA nor the GMMS procedure includes an explicit check to ensure the strongback enforces near-uniform drifts. Furthermore, while the spine is generally specified to remain elastic to avoid damage to it during a seismic event, its members are designed using the AISC *Specification* (AISC 2016a) and AISC *Seismic Provisions* (AISC 2016b), which provide no guarantee of truly elastic response.

The objectives of this work are to (1) determine how the performance of the frames produced by the design methods compare to one another; and (2) determine how the performance varies when the strength and stiffness of the strongback are varied. These objectives were achieved by designing frames according to both SMPA and GMMS, and comparing them to frames designed by standard linear response spectrum analysis according to ASCE 7-22 (ASCE 2022) with capacity design by AISC 341-16 (AISC 2016b). The frames were analyzed using nonlinear pushover, response history, and incremental dynamic analyses, with both nominal strength and stiffness as well as a range of modified strength and stiffness values for strongback members.

METHODS

Building Configurations

Three building configurations of varying heights (2, 4, and 8 stories), all using the same floor plan shown in Fig. 2, were investigated in this work. Elevation views are shown in Fig. 3. The seismic force resisting system consists of four total SBFs, two in each direction. The SBFs have a strongback occupying 1/3 the width of the bay; this configuration was identified by Simpson (2018) as reducing excessive inelastic demand on the beams and BRBs, without making the strongback too narrow. Each configuration was designed using the three design procedures, for a total of nine frame designs. The four SBFs and their tributary mass are the same regardless of orientation, so only one was designed and analyzed.

Gravity loads on the building were determined based on an assumed office occupancy, and are listed in Table 1. Member self-weight is included in the per-area dead load. Loads from the penthouse were "smeared" across the entire roof. No snow or wind loads were included in the design. Seismic hazard parameters were taken from the FEMA P695 seismic design category D_{max} (FEMA 2009). The buildings were assigned Risk Category II, for an importance factor I_e = 1.0 (ASCE 2022). Eccentricity due to accidental torsion was ignored.

Frame Design

The strongback braced frames for each of the three building configurations were designed following the procedures described in this section. These procedures were developed based primarily on current standards for design, such as ASCE 7-22 and AISC 360-16, and recommended approaches for design of spine frames, specifically, simplified modal pushover analysis (SMPA) and generalized modified modal superposition (GMMS). In some instances, additional decisions had to be made to cover cases not covered by current standards or recommended procedures, such as how to handle modeling the deformation-controlled beams in the equivalent linear model used by the GMMS procedure. These cases are described as they arise in the following sections.

The general process started with sizing the energy-dissipating components (i.e., the BRBs and the beams). Then, for trial designs, member strength evaluation was performed for non-capacity and capacity load combinations. Member sizes were selected through an iterative process to achieve least weight within the constraints. The selection of member sizes was manual, and a formal optimization was not performed. Seismic drift limits and stability coefficient checks from ASCE 7-22 (ASCE 2022) were also performed.

The frames consist of ASTM A992 wide-flange members with specified minimum yield strength F_y = 345 MPa (50 ksi) and expected yield strength R_yF_y = 380 MPa (55 ksi) for beams, columns, and conventional braces. The buckling-restrained braces have a specified yield strength of 290 MPa (42 ksi); stiffness factor Q = 1.4, which accounts for the additional stiffness due to the end regions; and hardening parameters β = 1.2 and ω = 1.46, which are used to determine the capacity-limited force from the BRB. The BRB hardening parameters are the same as used for the calibrated BRB model described by Simpson (2018). For design purposes, column splices were assumed to occur every two stories, but were not directly modeled in the analyses.

All analysis models used in this work, including those for design, were developed using OpenSees v3.4.0 (McKenna et al. 2010). Only the overview of each procedure and selected design variables are described here; full details are available online at https://doi.org/10.17603/ds2-jrcm-2c58.

Strength design

The initial phase of design consisted of sizing the energy-dissipating mechanisms of the frames—the core area A_{sc} of the BRBs and the member size of the beams—based on the equivalent lateral force (ELF) base shear.

The ELF base shear V was calculated using $R = 8$ (Simpson 2018). The approximate fundamental period T was calculated according to Eq. (1) following the guidelines from FEMA P695 (FEMA 2009):

$$T = \min(C_u C_t h_n^x, 0.25\text{ s}) \tag{1}$$

where C_u is the coefficient for the upper limit on calculated period from ASCE 7-22, equal to 1.4 for seismic design category D_{max} (ASCE 2022); C_t and x are approximate period coefficients from ASCE 7-22; and h_n

is the ground-to-level height of the roof in meters. For the strongback braced frames, values of C_t = 0.0731 (C_t = 0.03 when h_n is in feet) and x = 0.75 were selected due to the similarity to buckling-restrained braced frames.

To size the energy-dissipating mechanisms, the cross-sectional area of the BRB core was selected to be the same at each story. While standard braced frame design procedures call for BRBs to be sized proportional to the first-mode story shear profile, the elastic spine in SBFs offers the opportunity to use a single BRB size, simplifying construction and taking advantage of the ability of the strongback to redistribute internal forces (Simpson 2018). Assuming the strongback is stiff and strong enough to engage all levels of the structure fully, a uniform story drift profile is imposed, with corresponding uniform strain demands at all levels. Using the recommendation from Simpson (2018), the BRBs at each level were sized for a constant shear demand at each level equal to 80% of the ELF base shear. Since the first story is taller than the others, and thus the resultant axial force in the BRB is different, this method results in a different required steel core area $A_{sc,r}$ for different story heights. The average of the required area over the stories was used instead of the required area at each story to keep the BRB core area the same at each level. The actual core area sizes were selected to be the next 323 mm^2 (0.5 in.^{2}) above the required area; these design values are listed in Table 2.

Available member strengths for the force-controlled elements (columns and conventional braces) were determined using the effective length method with effective length factor, K = 1.0 (AISC 2016a). Axial, flexure, and axial-flexure interaction limit states were considered, according to AISC Specification Chapters E, F, and Section H1.1, respectively (AISC 2016a). Initial required strengths and sizes were determined from elastic second-order analysis under ELF loads, with final required strengths and sizes from the individual design procedures.

For non-capacity-limited load combinations, required strengths were determined using ASCE 7-22 Section 2.3.6 basic load combinations (6) and (7):

$$\begin{aligned} &1.2D + 0.5L + E_v + E_h \\ &0.9D - E_v + E_h \end{aligned} \tag{2}$$

where D is the dead load, L is the live load, E_v is the vertical earthquake load equal to $0.2S_{DS}D$, and E_h is the horizontal earthquake load, as determined by the specific analysis procedure. The gravity load portion of these load combinations was always directly included in the analysis. Load combination (6) usually calls for a 1.0 live load factor, but the use of 0.5 is permitted for distributed live loads less than or equal to 4.78 kPa (100 psf). Live load reduction was calculated in accordance with ASCE 7-22 (ASCE 2022) and applied to the model using the technique described by Ziemian and McGuire (1992). AISC 360-16 notional loads were included as 0.002 times the gravity load.

A two-dimensional second-order elastic model was used for determining ELF drifts and required strengths. The model consists of centerline beam-column elements with elastic fiber sections (to ensure that elastic properties remained the same between the ELF model and the models described later incorporating material nonlinearity). The BRBs were modeled with truss elements, with amplified elastic modulus QE_s.

The frames were also designed for capacity-limited demands and higher mode dynamic effects, using three different procedures to evaluate the differences between the procedures. The three procedures are 1) simplified modal pushover analysis, or SMPA (Simpson and Rivera Torres 2021); 2) generalized modified modal superposition, or GMMS (Martin and Deierlein 2021); and 3) linear response spectrum analysis according to ASCE 7-22 with capacity analysis by AISC 341-16, or RSAC (AISC 2016b; ASCE 2022).

Simplified modal pushover analysis

The SMPA procedure determines the forces on the spine through a combination of a displacement-controlled pushover analysis in mode 1 and load-controlled static analyses in higher modes.

Three models are required for the SMPA procedure: a pushover model with expected material strengths (used in mode 1), a pushover model with specified minimum material strengths (used in the higher modes), and an elastic design model (used for design criteria required to be determined by the equivalent lateral force procedure).

The pushover models used for SMPA, shown schematically in Fig. 4, are based on the numerical model developed by Simpson (2018), incorporating simplifications described by Simpson and Rivera Torres

(2021) for the "PP" configuration, where force-controlled actions are modeled as elastic responses, and displacement-controlled actions are modeled as elastic perfectly-plastic. The model uses centerline force-based beam-column elements with distributed plasticity, using two elements per member and five Gauss-Lobatto integration points per element. The BRBs are modeled using corotational truss elements with area equal to A_{sc} and modified elastic modulus equal to QE_s. The beams are connected to the columns with rotational springs representing the shear tabs. The connections have a moment strength of $0.3M_p$ at "bare" shear tabs and $0.7M_p$ at shear tabs that are partially restrained by a brace gusset plate, where M_p is the plastic moment strength of the beam (AISC 2016a). The shear tabs are assumed to yield at a rotation of 0.005 radians. Rigid offsets representing connection regions were incorporated for all members based on member geometry and the location of brace gusset plates. As specific gusset plate sizes were not designed or detailed, offsets based on a percentage of the workpoint-to-workpoint length were used instead. At member ends where a gusset plate would restrain the rotation, a rigid offset equal to 15% of the member length was used. At member ends where no gusset plate is present, a rigid offset representing the physical offset from the workpoint due to the connecting member's size was used (e.g., beams are offset from workpoints by half the column depth).

The SMPA procedure requires determination of target roof drifts, $\theta_{R,i}$, and target base shears, $V_{b,i}$, for each mode i up to a minimum of 95% modal mass participation. The first-mode displacement-controlled analysis only requires a target roof drift, while the force-controlled analyses in the higher modes use a target base shear as the primary target, with the target roof drift as a secondary limit indicating insufficient stiffness. The target values are determined from spectral displacements and eigenvalue analysis of the pushover model; see (Simpson and Rivera Torres 2021) for details on calculation of $\theta_{R,i}$ and $V_{b,i}$. These values are listed in Table 3.

The modal combination for SMPA response to determine E_h is given by

$$E_h = \pm\left(\left|r_1\right| + \sqrt{r_2^2 + \cdots + r_N^2}\right) \tag{3}$$

where r_i is the response (axial, shear, moment, etc.) to SMPA demands from mode i; and N is the number of modes being considered. Note that the signs of the individual responses are lost due to the modal combination.

Member sizes resulting from the SMPA procedure are shown in Table 4.

Generalized modified modal superposition

The GMMS procedure determines the forces on the spine using an equivalent linear model that represents the pivoting response of the spine at peak displacement under MCE-level shaking. Two models are required for the GMMS procedure: an equivalent linear model used to determine GMMS modal responses, and the elastic design model used for ELF design criteria.

The GMMS procedure uses an equivalent linear model to estimate the demands on the force-controlled elements by replacing the deformation-controlled elements with equivalent stiffness springs. An iterative procedure is used to estimate the roof drift ratio at MCE, θ_{MCE}, and an equivalent SDOF rotational stiffness, K_{eq}. The equivalent stiffness is equal to the secant stiffness M_{MCE}/θ_{MCE}, multiplied by the equivalent stiffness modification parameter λ; λ is based on a linear regression of rocking frame data, and may not be appropriately calibrated for SBFs, as they have different response characteristics to rocking frames. M_{MCE} is the estimated overturning moment at MCE, which, for SBFs, Martin and Deierlein (2021) recommend to be based on the capacity-limited forces in the BRBs. The stiffness of the individual equivalent stiffness springs is then determined by rational analysis, such that the global frame overturning stiffness is equal to K_{eq}. Response spectrum analysis, with a modified modal combination rule, is then used to apply forces to the equivalent model and determine required strengths.

The GMMS equivalent linear model for strongback braced frames as described by Martin and Deierlein (2021) does not include the secondary energy dissipation provided by beam bending at the face of the strongback. Initially for this work, the beams were to be modeled as force-controlled elements to stay consistent. However, initial design analysis showed that the beams could not be sized appropriately, as larger beams simply attracted more force. For this work, the procedure was modified to include equivalent stiffness rotational springs at the face of the strongback in order to model the beam yielding, as well as the standard equivalent stiffness springs for the BRBs. A schematic of the equivalent linear model is shown in Fig. 5.

The modal combination for GMMS responses to determine E_h is given by

$$E_h = \pm 1.3\left(\frac{|r_1|}{R_1} + \sqrt{r_2^2 + \cdots + r_N^2}\right) \tag{4}$$

where R_1 is the GMMS reduction factor for mode 1, which for unstacked frames is equal to the GMMS equivalent stiffness modification parameter λ; r_i is the response to GMMS demands from mode i; N is the number of modes being considered; and the 1.3 factor comes from the suggested load combination for GMMS (Martin and Deierlein 2021). No specific number of modes or level of modal mass participation is specified in the description of the GMMS procedure; for consistency with SMPA, the same number of modes were considered. Design variables for the GMMS procedure are shown in Table 5.

Member sizes resulting from the GMMS procedure are shown in Table 6.

Response spectrum analysis with capacity design

To provide a control case based on current seismic design practice, a response spectrum analysis with capacity design (RSAC) procedure was used. The RSAC procedure requires two models: the elastic design model, used for the response spectrum analysis and ELF design criteria, and a capacity design model, where the BRBs and beam plastic hinges (at the face of the strongback) are replaced with equivalent capacity-limited forces and moments. The capacity design model, shown schematically in Fig. 6, only incorporates the effects from mode 1. Capacity-limited BRB forces in compression, P_c, and in tension, P_t, were calculated using the equations from AISC 341-16 (AISC 2016b):

$$\begin{aligned} P_c &= \omega\beta R_y F_{ysc} A_{sc} \\ P_t &= \omega R_y F_{ysc} A_{sc} \end{aligned} \tag{5}$$

where ω and β are the BRB hardening parameters, $R_y F_{ysc}$ is the expected yield strength of the steel core = 42 ksi, and A_{sc} is the area of the steel core. Capacity-limited moments from the beams were conservatively assumed to be equal to the full expected plastic moment $M_{pe} = R_y F_y Z_x$, where $R_y = 1.1$ for ASTM A992 members (AISC 2016b).

Member sizes resulting from the RSAC procedure are listed in Table 7.

Other design checks

Beam, column, and conventional brace members were also designed to satisfy ductility requirements from AISC 341-16. SBFs have not yet been codified in AISC 341-16, so the required ductility categories were selected based on the expected role of the members. Since the beams form part of the energy dissipation system, they were selected to be highly ductile members, while columns and braces were selected to be moderately ductile since they are intended to remain elastic.

The equivalent lateral force procedure with $C_d = 5$ was used to check the ASCE 7-22 limits on stability coefficient θ and story drift Δ. This is the same C_d as for buckling-restrained braced frames (ASCE 2022), since SBFs have not been assigned performance factors. The stability coefficient was calculated using Eq. (G19-2) from (Charney et al. 2020), where two analyses are performed, one with P-Δ effects included and one without. Simple limits of $\theta_{max} = 0.1$ and $\Delta_a = 0.02h_s$ were used. The only case where stability checks controlled the design was RSAC-8, where story drift limits were exceeded in the intermediate stories under a purely strength-based design.

Nonlinear Analysis

To evaluate the resulting designs, nonlinear static pushover and nonlinear dynamic analyses were performed. Three performance variables for the strongback were investigated: (1) resistance to collapse, measured by the collapse margin ratio calculated from incremental dynamic analysis; (2) ability to distribute drift demands across stories under MCE-level shaking, measured using the maximum "marginal drift"; and (3) ability of the strongback to remain elastic under MCE-level shaking, measured using the total strain energy absorbed by the strongback over the duration of the ground motion. To investigate the required strength and stiffness of the strongback, and to evaluate how the different design methods compare to each other, these variables were measured for a range of stiffness and strength modifications made to the strongback members. While these performance variables do not directly measure resilience, they are used in this study as surrogate metrics to quantify the effect of strongback parameters and design on the system's resilience to structural damage. Each of them is related to resilience: for example, a structure not collapsing or otherwise being less damaged can enable a quicker return to normal operation after a seismic event.

The model used for the nonlinear analyses is similar to the one used for the SMPA design procedure (Fig. 4), but incorporates additional sources of nonlinearity. Wide-flange members were represented using centerline beam-column elements using the force-based formulation, 5 integration points per element, and 2 elements per member, with fiber cross sections utilizing the Steel02 uniaxial material model. Residual stresses were incorporated for wide-flange members using the Lehigh pattern (Galambos and Ketter 1959). Buckling restrained braces were represented using truss elements with a Steel4 non-symmetric hysteretic model and Fatigue wrapper, with parameters taken from the BRB material model calibration in (Simpson 2018). All materials used the expected yield strength R_yF_y for the "nominal" yield stress. Geometric nonlinearity was incorporated using corotational truss elements and a corotational transformation for the beam-column elements. Both the strongback base and the opposite column base were modeled as pinned. Tributary gravity loads equal to $1.05D + 0.25L$ were lumped at brace workpoints. Mass based on $1.0D$ was distributed in the same fashion as the gravity loads. P-Δ effects were included through leaning columns which carried the remaining gravity load not directly tributary to the frame. The leaning columns were connected to the rest of the frame by constraining their lateral displacements to the corresponding workpoint.

To investigate the effect of the strongback's strength and stiffness, the strongback members (here comprising the strongback column as well as the diagonal and tie braces, but excluding the beams) were modeled with varying yield strength F_y and elastic modulus E. F_y and E were selected as the parameters for the strongback's strength and stiffness due to their ease of modification and, in contrast to cross-section properties, their relative ability to decouple strength and stiffness. A range between 0.1 and 10 times as stiff or strong was identified as the range of interest through preliminary analysis. Further analysis showed that significant strength reduction led to poor, unrealistic seismic performance, so a range between 0.6 and 10 times was utilized when varying strength. A total of 810 frames were evaluated: the 9 base designs were evaluated at nominal strength and stiffness, with 34 values of strength and stiffness varied together, 29 values of stiffness varied alone, and 26 values of strength varied alone.

The collapse performance of the overall structure was measured using incremental dynamic analyses (IDA), following the FEMA P695 methodology, to determine the adjusted collapse margin ratio, *ACMR*, for each configuration. An *ACMR* of 1.0 indicates a 50% probability of collapse at the MCE intensity, with increasing values of *ACMR* corresponding to decreasing probability of collapse. Following FEMA P695 Appendix F for collapse evaluation of individual buildings, a 10% probability of collapse at MCE was considered the minimum acceptable collapse performance, evaluated by comparing the *ACMR* to the minimum acceptable *ACMR* for a 10% probability of collapse, $ACMR_{10\%}$. Collapse was not directly simulated, and instead defined using a story drift limit of 5%. This limit is based on experimental tests of column drift capacities, which showed capacities of 7–9% (Newell and Uang 2006), and conservative estimates of braced frame drift capacities (Uriz and Mahin 2008). A full FEMA P695 study requires identification of performance groups and a broader set of configurations than investigated here; this study is thus strictly a subset of a full FEMA P695 study of strongback braced frames.

The strongback's ability to distribute demands under MCE-level shaking was measured using the maximum "marginal drift" *L*. Here, marginal drift is defined as the difference between the story drift ratio and the average story drift ratio of the other stories. The maximum value of this marginal drift is defined by Eq. (6):

$$L = \max_{i,t}\left(\theta_i(t) - \frac{1}{N-1}\sum_{j=1,\, j\neq i}^{N}\theta_j(t)\right) \tag{6}$$

where $\theta_i(t)$ is the absolute value of the story drift ratio at story *i* and time *t*, and *N* is the number of stories. This measure identifies when drift concentrations occur, and avoids misleading results that can occur at small drift levels.

The strongback's ability to remain elastic under MCE-level shaking was measured using the total energy absorbed by the strongback members through deformation, calculated cumulatively over the duration of the ground motion. The total energy was calculated from element-level forces and deformations, which has the limitation of including elastic energy from locked-in stresses. The elastic contribution to the strain energy is small relative to the plastic and hardening contributions at the MCE-level shaking considered. A primary goal of the strongback is to remain elastic and limit damage under severe shaking to specified locations in the frame (i.e., the primary energy dissipation mechanism); if significant yielding and hardening occurs, then the strongback may need to be repaired as well. Furthermore, detailing requirements for SBFs have not been established—if significant yielding occurs in the strongback, requirements should be established to ensure a ductile global response.

Nonlinear static pushover analysis

Nonlinear static pushover analysis was used to identify the period-based ductility, μ_T, of the frames. This quantity is required to determine the spectral shape factor, *SSF*, and the total system uncertainty, β_{TOT}, which are used in the FEMA P695 collapse evaluation procedure (FEMA 2009).

The pushover analysis was performed using a first-mode distribution of lateral forces

$$f_i \propto m_i \phi_i \tag{7}$$

where m_i is the mass at node i and ϕ_i is the x-direction eigenvector for mode 1 at node i (determined by eigenvalue analysis of the model), until a drop in force of 20% was detected. The maximum base shear V_{max} and the ultimate displacement δ_u were recorded. V_{max} was used to calculate the effective yield displacement $\delta_{y,eff}$ per FEMA P695 Eq. (6-7) and (6-8). μ_T is then defined as the ratio of δ_u to $\delta_{y,eff}$.

Due to convergence issues, not all pushover analyses reached the specified 20% drop in force. These convergence issues were associated with BRB fracture. Thus, it was concluded that the failed analyses still accurately captured V_{max} and $\delta_{y,eff}$, but may underpredict δ_u and μ_T (e.g., if a single BRB fracture does not result in a 20% drop in strength). Values of μ_T are high enough, however, that this potential underprediction does not impact the results, as *SSF* is constant with respect to μ_T when $\mu_T > 8.0$ and β_{TOT} is constant with respect to μ_T when $\mu_T > 3.0$, and all the analyses that potentially underpredict μ_T have $\mu_T > 8.0$.

Nonlinear dynamic analysis

Response history analyses and incremental dynamic analyses were performed using the 22 ground motion pairs of the FEMA P695 far-field record set, which provides a set of site-independent strong ground motions suitable for collapse evaluation (FEMA 2009). The ground motions were scaled as shown in Eq. (8):

$$\ddot{x}_g = SF \cdot \frac{S_{MT}}{\hat{S}_{NRT}} \cdot NM \cdot \ddot{x}_{g,recorded} \tag{8}$$

where SF is a selectable scale factor, S_{MT} is the spectral intensity of the MCE at the fundamental period of the building, $\hat{S}_{NRT}$ is the median spectral intensity of the normalized record set at the fundamental period of the building, and NM is the normalization factor for the specific ground motion. NM is calculated for each ground motion as the median peak ground velocity (PGV) of the record set divided by the PGV of the ground motion. The fundamental period used for calculation of these values is the approximate fundamental period listed in Table 2. Values of $S_{MT} / \hat{S}_{NRT}$ and NM are tabulated in FEMA P695, and a value of $SF = 1.0$ provides the ground motion scaled to MCE. For incremental dynamic analysis, SF was increased until collapse was detected (using the non-simulated collapse limit of 5% story drift).

Using the results of the IDAs, the adjusted collapse margin ratio, $ACMR$, was determined. $ACMR$ is the product of the collapse margin ratio, CMR, and the spectral shape factor, SSF, as defined in FEMA P695 (FEMA 2009). The collapse margin ratio is the ratio of the median collapse intensity $\hat{S}_{CT}$ to the intensity of the maximum considered earthquake S_{MT}. Given the scaling used in this work (Eq. (8)), the collapse margin ratio is equal to the scaling factor, SF, that results in half the ground motions causing collapse.

The spectral shape factor, SSF, depends on the record set, the fundamental period of the building (Table 2), seismic design category, and the period-based ductility, μ_T, determined from static pushover analysis. Values of SSF are tabulated in FEMA P695 Table 7-1 (FEMA 2009).

Calculating the acceptable $ACMR$ for a 10% collapse probability, $ACMR_{10\%}$, requires an assessment of uncertainty in the evaluation. This requires rating the quality of (1) the nonlinear model, (2) the design requirements, and (3) the available test data. For this work, all "good" ratings were used. The nonlinear model captures important collapse-related behaviors (e.g., P-Δ, BRB fracture, yielding and residual stresses), but does not capture all potentially collapse-related behavior (e.g., fracture of conventional braces or connections). The design requirements are based in sound principle and build from well-established requirements for structural steel systems, but aspects specific to strongback systems have not been significantly tested. Significant amounts of test data exist for the individual components, though full-scale testing of strongbacks is limited. While other system uncertainty ratings could be justifiable, these selections are similar to previous SBF studies and align with previous FEMA P695 studies (Korlapati et al. 2021; Simpson 2018). The final component of the uncertainty is the record-to-record variability, which is constant when $\mu_T \geq 3.0$. Given these ratings, and since $\mu_T \geq 3.0$ for all configurations, the total system collapse uncertainty $\beta_{TOT} = 0.525$. This gives an acceptable value of the adjusted collapse margin ratio for a 10% collapse probability, $ACMR_{10\%}$, of 1.96.

RESULTS AND DISCUSSION

The presentation of results and discussion thereof is divided into topics of collapse resistance, distribution of demands, and strongback inelasticity. The plots in Fig. 7–Fig. 9 show the median value of the frame responses when subjected to the 22 ground motion pairs of the FEMA P695 far-field record set.

Collapse Resistance

The plots in Fig. 7 show the adjusted collapse margin ratio, *ACMR*, for the frames as a function of the modulus of elasticity, E, and steel yield stress, F_y, used for the strongback members, as well as the acceptable value of the adjusted collapse margin ratio for a 10% collapse probability, $ACMR_{10\%}$, of 1.96, plotted as a horizontal dot-dashed line.

At nominal strength and stiffness, the design methods provide acceptable collapse performance (i.e., $ACMR \geq ACMR_{10\%}$) except for the 4-story frame designed using the RSAC method. The RSAC method is a simple method that captures higher-mode effects and yield mechanisms independently; it is used in this work as a point of comparison to the other methods that more rigorously capture these behaviors and their interaction, including partial yield mechanisms. That the RSAC method provides sufficiently collapse-resistant designs for the 2- and 8-story frames indicates the novel design methods (i.e., SMPA and GMMS) are not necessary to provide collapse resistance for all SBF configurations. Furthermore, the results indicate that the 4-story frame occupies a "mid-range" where the combination of higher-mode effects and partial yielding mechanisms—a combination not accounted for by RSAC—is substantial. This is especially noted by the smaller column sizes produced by the RSAC method, for which the SMPA and GMMS methods predict significantly higher moment demands. Investigation of a broader range of frames is necessary to confirm the existence of this mid-range for SBFs in general.

The 8-story frames all have similarly high collapse resistance, with $ACMR$ exceeding $ACMR_{10\%}$ by 50% at nominal strength and stiffness for all three methods. The 8-story RSAC-designed frame is notably different from the other 8-story frames, despite providing equivalent collapse performance. RSAC-8 was controlled by drift limits, leading to larger member sizes than would have been obtained from strength design alone (the frames designed by the other methods were not controlled by drift limits). The RSAC frames also consistently have larger opposite columns than strongback columns; while this is also seen in SMPA-2 and SMPA-4, the difference is larger in the RSAC frames.

$ACMR$ increases when increasing strongback stiffness and strength together. For the 2- and 4-story buildings, a plateau is reached at 2-3 times the nominal strength and stiffness. For the 8-story buildings, no plateau is observed within the ratios investigated. Increasing strength or stiffness individually also provides benefit. The collapse resistance is more sensitive to changes in strength than stiffness, though very large increases in strength provide less benefit proportionally and eventually reach a plateau at 2-7 times the nominal strength. Changes to stiffness affect the results across the entire range.

The fact that collapse resistance varies, especially with strongback strength, indicates that the strongback with nominal E and F_y does not remain elastic at the median collapse intensity. This is expected in part because the design methods target elastic behavior at MCE, not collapse. If the strongback were stronger, such that it did remain elastic, the collapse resistance would increase by as much as 78% (in the case of RSAC-4). The $ACMR$ for the stronger strongback is significantly higher than the acceptable value, $ACMR_{10\%}$; this implies, for example, that fewer or smaller BRBs could be used with a stronger strongback while still achieving the desired collapse performance. However, using smaller BRBs decreases the demands on the strongback predicted by the design methods. Thus, the design methods investigated here for the strongback are satisfactory only for the BRBs sizes generated by the initial assumptions about the strongback, and not for the general case of arbitrary BRB sizes and distributions. Further work is needed to develop rigorous and broadly applicable BRB size selection criteria.

With nominal parameters, and generally across the parameter range, the 2- and 4- story GMMS frames have higher collapse resistance than the other design methods; this is expected because the GMMS-designed frames have bigger members (see Table 8). For the 8-story configuration, the GMMS frame performs very similarly to the SMPA frame. With the exception of the 0.1 stiffness factor in the 4-story building, $ACMR$ is greater than $ACMR_{10\%}$ for all variations of the GMMS frames, indicating that GMMS produces larger members than necessary for SBFs; thus, details of the method, such as the 1.3 factor in Eq. (4), could be revisited for SBFs.

Distribution of Demands under MCE-level Shaking

One of the defining features of a strongback is its ability to more uniformly distribute demands along the height of the building. The strongback's ability to distribute demands under MCE-level shaking is shown in Fig. 8. The median value at MCE of the maximum marginal drift—see Eq. (6)—is plotted.

For all buildings and design methods, except for RSAC-4, the marginal drift remains the same when strength is increased from nominal, indicating that only minimal yielding is occurring at MCE in the strongback in the other frames at nominal strength and stiffness. Marginal drift will increase rapidly when strength is reduced sufficiently, indicating failure of the strongback to maintain vertical continuity and the formation of a soft story. This increase in marginal drift was not observed for the GMMS frames, but it is reasonable to assume that it would see the same rapid increase in maximum marginal drift if strength was decreased further. This further indicates that the GMMS procedure produces larger members than necessary.

Changing stiffness corresponds to changes in marginal drift across the entire range of factors investigated. Decreasing stiffness increases marginal drifts, though not as rapidly as decreasing strength.

Increasing stiffness reduces marginal drifts, approaching zero marginal drift at 10 times nominal stiffness, indicating near-uniform drifts over the entire duration of the ground motion.

Changing stiffness and strength together simply shows a combination of the above behaviors, with reductions in strength and stiffness compounding with each other.

For the 2-story building, the RSAC and SMPA methods result in similar median behavior, while GMMS has slightly lower marginal drifts. For the 8-story building, all design methods provide similar behavior over the whole range of factors investigated, with GMMS and SMPA providing nearly identical median results while RSAC performs slightly worse than the novel design methods. The similarity of the GMMS and SMPA results can be attributed to the similarity of the strongback members, especially the strongback braces, which are the primary contributor to the shear-type response of the strongback.

Strongback Inelasticity under MCE-level Shaking

Strongbacks are expected to remain essentially elastic under ground shaking at the MCE level. The strongback's ability to remain elastic under MCE-level shaking is shown in Fig. 9 as the ratio of the strain energy absorbed by the strongback to the total strain energy absorbed by the frame. As noted previously, this measure includes some amount of "locked-in" elastic energy, but the dominant source is dissipation through yielding.

At nominal strength and stiffness, the strain energy absorbed by the strongback is less than 1% of the strain energy absorbed by the frame as a whole (except for RSAC-4, which is ~5%). The strain energy ratio increases rapidly with reductions in strength, while increases in strength provide only marginal reductions. When increasing stiffness alone, the share of the strain energy in the strongback tends to increase. As the strain energy decreases when increasing both strength and stiffness, the increase with stiffness alone is not attributable simply to large amounts of stored elastic energy, and is indicative of the stiffer strongback attracting greater demands.

Comparing design procedures, the control design method (RSAC) shows more yielding in the strongback across all building heights and modifications. GMMS generally shows less yielding, though

GMMS and SMPA show very similar behavior for the 8-story structure. This indicates that the novel design methods are more effective at producing designs that remain essentially elastic during MCE-level shaking.

Other Results

For brevity, the results shown in this section are for a subset of the frames; complete figure sets are available online at https://doi.org/10.17603/ds2-jrcm-2c58.

Fig. 10 shows the median strain energy absorbed by all the components of the 2-, 4-, and 8-story SMPA frames at MCE, grouped by element type. As expected, the BRBs are the primary source of energy dissipation, far exceeding the combined contribution of the other elements. The beams, despite being designated as a secondary energy dissipator, do not contribute significantly to the energy dissipation of the frames. For the 2- and 4-story frames at nominal strength and stiffness, the strongback, which is designed to remain essentially elastic, absorbs as much energy as the beams; noting that the strongback is significantly larger and thus has much more strain energy capacity. Similar results are seen for the frames designed by the other design methods.

Fig. 11 shows the median strain energy ratios of the different elements of the strongback itself at MCE. The diagonal braces are the most significantly affected by changes to strongback strength and stiffness. At low strength and stiffness, large buckling deformations lead to significant increases in the strain energy handled by the braces. This indicates that, for these frames, as the strongback becomes stiffer and stronger, the response transitions from a shear-dominated response to a flexure-dominated response. Notably, the ties do not contribute significantly to the dissipation in the strongback. Similar results are seen for the frames designed by the other design methods.

Fig. 12 shows median values of the maximum residual story drift at MCE for all the frames when varying strength and stiffness together. The maximum residual story drift was taken as the maximum value of the drift at each story at the end of the analysis, with time allowed at the end of the ground motion (equal to 10% of the ground motion duration) for the model to settle. The design methods all provide acceptable residual drift control at nominal strength and stiffness, with median residual drifts under 1%. Similar to story drift concentration, reductions in strength and stiffness quickly lead to large increases in residual drift. The residual drifts of the GMMS frames are largely insensitive to changes in strength and stiffness over the range investigated. Overall, the SBFs are very capable at controlling residual drift, indicating their usefulness in improving resilience to seismic events.

CONCLUSIONS

In this work, three design methods for strongback braced frames were evaluated for three buildings of varying heights. The design methods were evaluated using nonlinear analysis across a range of modifications to the strength and stiffness of the resulting frames. The methods were evaluated for their ability to (1) provide collapse resistance, (2) limit story drift concentrations at MCE, and (3) limit yielding in the strongback spine itself at MCE. The results show that there is utility in the use of novel design methods for the design of strongback braced frames. The key observations from this work are:

- The simplified modal pushover analysis (SMPA) and generalized modified modal superposition (GMMS) procedures are generally well-calibrated and provide value above the simpler response spectrum analysis with capacity design (RSAC).
- Frames designed according to SMPA and GMMS have acceptable *ACMR*, and the strongback behaves as expected with minimal drift concentration and yielding.
- GMMS is more conservative, resulting in a heavier strongback, but also improved performance. The 1.3 factor on the GMMS loads—see Eq. (4)—could be revisited for strongbacks.
- For all measures observed in this study, the greatest impact was from not having enough strength in the strongback. Reductions in strongback strength led to rapid loss of collapse resistance, and large increases in drift concentration and strongback inelasticity at MCE-level shaking. With the exception of RSAC-4, the frames saw minimal benefit to MCE-level responses when strength was increased from nominal. All frames saw reductions in story drift concentrations from increased stiffness, but increased stiffness also led to increased strongback yielding, especially for RSAC-4 and RSAC-8.

- The BRBs, as expected, provide the vast majority of the energy dissipation in the structure. The beams, despite being designated as secondary energy dissipators, do not provide large amounts of energy dissipation.

Overall, this work furthers the development of the SBF system as a viable seismic force-resisting system for highly resilient buildings. Several lines of inquiry for future work remain, including:

- Further work is needed to develop rigorous and broadly applicable BRB size selection criteria. While the SMPA and GMMS design methods can provide good predictions of the strongback demands, they are reliant on the initial BRB design step in order to provide sufficient lateral resistance. Prediction of strongback demands and selection of BRB sizes are inherently coupled, but the current methods for selecting BRB size for SBFs rely on assumptions about the overall frame behavior that cannot be applied to generalized BRB distributions.
- Further work is needed to clarify the role of the beams in strongback braced frames and to develop criteria for sizing beams in strongback braced frames.

DATA AVAILABILITY STATEMENT

All data, models, and code generated or used during the study are available in a repository online at https://doi.org/10.17603/ds2-jrcm-2c58 in accordance with funder data retention policies.

ACKNOWLEDGMENTS

This material is based upon work supported by the National Science Foundation under Grant No. 1940197. Any opinions, findings, and conclusions or recommendations expressed in this material are those of the author(s) and do not necessarily reflect the views of the National Science Foundation. The computation for this work was performed on the University of Tennessee Infrastructure for Scientific Applications and Advanced Computing (ISAAC) computational resources.

REFERENCES

Abolghasemi, S., N. E. Wierschem, and M. D. Denavit. 2024. “Impact of strongback on structure with varying damper and stiffness irregularity arrangements.” *Journal of Constructional Steel Research*, 213: 108333. https://doi.org/10.1016/j.jcsr.2023.108333.

AISC. 2016a. *Specification for structural steel buildings*. Chicago, Illinois: American Institute of Steel Construction.

AISC. 2016b. *Seismic provisions for structural steel buildings*. Chicago, Illinois: American Institute of Steel Construction.

ASCE. 2017. *Seismic evaluation and retrofit of existing buildings*. Reston, Virginia: American Society of Civil Engineers.

ASCE. 2022. *Minimum design loads and associated criteria for buildings and other structures*. Reston, Virginia: American Society of Civil Engineers.

Bosco, M., E. M. Marino, and P. P. Rossi. 2018. “A design procedure for pin-supported rocking buckling-restrained braced frames.” *Earthquake Engng Struct Dyn*, 47 (14): 2840–2863. https://doi.org/10.1002/eqe.3112.

Broujerdian, V., and E. Mohammadi Dehcheshmeh. 2022. “Locating the rocking section in self-centering bi-rocking walls to achieve the best seismic performance.” *Bull Earthquake Eng*, 20 (5): 2441–2468. https://doi.org/10.1007/s10518-022-01325-y.

Bruneau, M., and A. Reinhorn. 2006. “Overview of the resilience concept.” *Proceedings of the 8th U.S. National Conference on Earthquake Engineering*. San Francisco, California.

Charney, F. A., T. F. Heausler, and J. D. Marshall. 2020. *Seismic loads: guide to the seismic load provisions of ASCE 7-16*. Reston, Virginia: American Society of Civil Engineers.

Chopra, A. K., and R. K. Goel. 2002. “A modal pushover analysis procedure for estimating seismic demands for buildings.” *Earthq Engng Struct Dyn*, 31 (3): 561–582. https://doi.org/10.1002/eqe.144.

Eatherton, M. R., X. Ma, H. Krawinkler, G. G. Deierlein, and J. F. Hajjar. 2014. “Quasi-static cyclic behavior of controlled rocking steel frames.” *J. Struct. Eng.*, 140 (11): 04014083. https://doi.org/10.1061/(ASCE)ST.1943-541X.0001005.

FEMA. 2009. *Quantification of building seismic performance factors*. Federal Emergency Management Agency.

Galambos, T. V., and R. L. Ketter. 1959. “Columns under combined bending and thrust.” *J. Engrg. Mech. Div.*, 85 (2): 1–30. https://doi.org/10.1061/JMCEA3.0000084.

Gioiella, L., E. Tubaldi, F. Gara, L. Dezi, and A. Dall’Asta. 2018. “Modal properties and seismic behaviour of buildings equipped with external dissipative pinned rocking braced frames.” *Engineering Structures*, 172: 807–819. https://doi.org/10.1016/j.engstruct.2018.06.043.

Korlapati, S. C. R., R. Raman, and M. Bruneau. 2021. “Modeling and test data uncertainty factors used in prior FEMA P695 studies.” *J. Struct. Eng.*, 147 (2): 06020009. https://doi.org/10.1061/(ASCE)ST.1943-541X.0002906.

Kurama, Y., S. Pessiki, R. Sause, and L.-W. Lu. 1999. “Seismic behavior and design of unbonded post-tensioned precast concrete walls.” *PCI Journal*, 44 (3): 72–89. https://doi.org/10.15554/pcij.05011999.72.89.

Lai, J.-W., and S. A. Mahin. 2014. “Strongback system: A way to reduce damage concentration in steel-braced frames.” *Journal of Structural Engineering*, 141 (9): 04014223.

Martin, A., and G. G. Deierlein. 2021. “Generalized modified modal superposition procedure for seismic design of rocking and pivoting steel spine systems.” *Journal of Constructional Steel Research*, 183: 106745. https://doi.org/10.1016/j.jcsr.2021.106745.

Martin, A., G. G. Deierlein, and X. Ma. 2019. “Capacity design procedure for rocking braced frames using modified modal superposition method.” *J. Struct. Eng.*, 145 (6): 04019041. https://doi.org/10.1061/(ASCE)ST.1943-541X.0002329.

McKenna, F., M. H. Scott, and G. L. Fenves. 2010. "Nonlinear finite-element analysis software architecture using object composition." *J. Comput. Civ. Eng.*, 24 (1): 95–107. https://doi.org/10.1061/(ASCE)CP.1943-5487.0000002.

Newell, J., and C.-M. Uang. 2006. *Cyclic behavior of steel columns with combined high axial load and drift demand*. San Diego, California: University of California, San Diego.

Palermo, M., V. Laghi, G. Gasparini, S. Silvestri, and T. Trombetti. 2021. "Seismic design and performances of frame structures connected to a strongback system and equipped with different configurations of supplemental viscous dampers." *Front. Built Environ.*, 7: 748087. https://doi.org/10.3389/fbuil.2021.748087.

Priestley, M. J. N., and A. Amaris. 2003. "Dynamic amplification of seismic moments and shear forces in cantilever walls." *Proceedings of the FIB Symposium*, 196–197. Athens.

Priestley, M. J. N., R. J. Evison, and A. J. Carr. 1978. "Seismic response of structures free to rock on their foundations." *BNZSEE*, 11 (3): 141–150. https://doi.org/10.5459/bnzsee.11.3.141-150.

Priestley, M. J. N., S. (Sri) Sritharan, J. R. Conley, and S. Stefano Pampanin. 1999. "Preliminary results and conclusions from the PRESSS five-story precast concrete test building." *PCI Journal*, 44 (6): 42–67. https://doi.org/10.15554/pcij.11011999.42.67.

Roke, D. A. 2010. "Damage-free seismic-resistant self-centering concentrically-braced frames." Ph.D. Dissertation. Lehigh University.

Roke, D., R. Sause, J. M. Ricles, and N. Gonner. 2009. "Design concepts for damage-free seismic-resistant self-centering steel concentrically braced frames." *Structures Congress 2009*.

Simpson, B. G. 2018. "Design development for steel strongback braced frames to mitigate concentrations of damage." Ph.D. Dissertation. University of California, Berkeley.

Simpson, B. G. 2020. "Higher-mode force response in multi-story strongback-braced frames." *Earthquake Engng Struct Dyn*, 49 (14): 1406–1427. https://doi.org/10.1002/eqe.3310.

Simpson, B. G., and S. A. Mahin. 2018. "Experimental and numerical investigation of strongback braced frame system to mitigate weak story behavior." *Journal of Structural Engineering*, 144 (2): 04017211. https://doi.org/10.1061/(ASCE) ST.1943-541X.0001960.

Simpson, B. G., and D. Rivera Torres. 2021. "Simplified modal pushover analysis to estimate first- and higher-mode force demands for design of strongback-braced frames." *J. Struct. Eng.*, 147 (12): 04021196. https://doi.org/10.1061/(ASCE)ST.1943-541X.0003163.

Steele, T. C., and L. D. A. Wiebe. 2016. "Dynamic and equivalent static procedures for capacity design of controlled rocking steel braced frames." *Earthquake Engng Struct. Dyn.*, 45 (14): 2349–2369. https://doi.org/10.1002/eqe.2765.

Tremblay, R. 2003. "Achieving a stable inelastic seismic response for multi-story concentrically braced steel frames." *Engineering Journal*, 40 (2): 111–129.

Uriz, P., and S. A. Mahin. 2008. *Toward earthquake-resistant design of concentrically braced steel-frame structures*.

Wiebe, L., and C. Christopoulos. 2009. "Mitigation of higher mode effects in base-rocking systems by using multiple rocking sections." *Journal of Earthquake Engineering*, 13 (S1): 83–108. https://doi.org/10.1080/13632460902813315.

Wiebe, L., and C. Christopoulos. 2015. "A cantilever beam analogy for quantifying higher mode effects in multistorey buildings." *Earthquake Engng Struct. Dyn.*, 44 (11): 1697–1716. https://doi.org/10.1002/eqe.2549.

Ziemian, R. D., and W. McGuire. 1992. "A method for incorporating live load reduction provisions in frame analysis." *Engineering Journal*, 29 (1): 1–3.

FIGURE CAPTION LIST

- Fig. 1. Strongback braced frame. Shaded region indicates the members comprising the strongback.
- Fig. 2. Floor plan. Dashed lines indicate location of SBFs. Shaded area indicates location of penthouse.
- Fig. 3. Elevation view of SBFs.
- Fig. 4. Schematic of pushover model for SMPA procedure.
- Fig. 5. Schematic of equivalent linear model for GMMS procedure.
- Fig. 6. Schematic of capacity design model to accompany response spectrum analysis.
- Fig. 7. Adjusted collapse margin ratio. (a) Varying strength and stiffness; (b) varying stiffness, F_y remains nominal; (c) varying strength, E remains nominal. Left-to-right: 2, 4, and 8 stories
- Fig. 8. Story drift concentration at MCE, measured by maximum marginal drift. (a) Varying strength and stiffness; (b) varying stiffness, F_y remains nominal; (c) varying strength, E remains nominal. Left-to-right: 2, 4, and 8 stories
- Fig. 9. Strain energy stored in and dissipated by the strongback at MCE, as a ratio of the total frame strain energy. (a) Varying strength and stiffness; (b) varying stiffness, F_y remains nominal; (c) varying strength, E remains nominal. Left-to-right: 2, 4, and 8 stories
- Fig. 10. Median strain energy stored in and dissipated by the various components of the SMPA frames at MCE, varying strength and stiffness together. Left-to-right: 2, 4, and 8 stories
- Fig. 11. Median strain energy stored in and dissipated by the components of the strongback in the SMPA frames at MCE, varying strength and stiffness together. Left-to-right: 2, 4, and 8 stories
- Fig. 12. Median value of maximum residual drift at MCE, varying strength and stiffness together. Left-to-right: 2, 4, and 8 stories

TABLES

Table 1: Per-area gravity loads. Roof loads include “smeared” penthouse load.

Load Type	**Typ. Floor [kPa (psf)]**	**Roof [kPa (psf)]**
Dead	3.83 (80)	3.76 (78.5)
Dead (Wall/Parapet)	1.20 (25)	1.20 (25)
Live	3.83 (80)	0.800 (16.7)
Partition	0.718 (15)	—
Roof Live	—	0.397 (18.3)

Table 2: Initial design values

Number of Stories	**Approximate Period, T [s]**	**ELF Base Shear, V [kN (kip)]**	**Required BRB Size, $A_{sc,r}$ [mm^2 (in.^{2})]**	**BRB Size, A_{sc} [mm^2 (in.^{2})]**
2	0.578	1190 (268)	4630 (7.18)	4840 (7.5)
4	0.939	1530 (344)	5980 (9.27)	6130 (9.5)
8	1.55	1860 (418)	7200 (11.2)	7420 (11.5)

Table 3: Target roof drifts and base shears for SMPA procedure.

Building	**Mode**	**Target roof drift, $\theta_{R,i}$ [%]**	**Target base shear, $V_{b,i}$ [kN (kip)]**
SMPA-2	1	1.20	—
	2	0.0289	673 (151)
SMPA-4	1	1.04	—
	2	0.0591	2810 (631)
	3	0.00757	404 (90.8)
	4	0.000204	41.8 (9.39)
SMPA-8	1	0.987	—
	2	0.106	6400 (1440)
	3	0.0125	1550 (348)
	4	0.00118	75.0 (16.9)

Table 4: Member sizes for frames determined using the SMPA procedure.

Building	**Story**	**BRB Size [mm^2 (in.^{2})]**	**Beam**	**Left Column**	**Strongback Brace**	**Strongback Column**	**Tie Brace**
SMPA-2	1	4840 (7.5)	W12×96	W12×72	W12×96	W12×53	—
	2	4840 (7.5)	W12×96	W12×72	W12×53	W12×53	—
SMPA-4	1	6130 (9.5)	W12×96	W12×170	W12×210	W12×170	—
	2	6130 (9.5)	W12×96	W12×170	W12×79	W12×170	W12×106
	3	6130 (9.5)	W12×96	W12×96	W12×79	W12×79	W12×106
	4	6130 (9.5)	W12×96	W12×96	W12×79	W12×79	—
SMPA-8	1	7420 (11.5)	W12×120	W14×426	W14×426	W14×500	—
	2	7420 (11.5)	W12×120	W14×426	W14×342	W14×500	W14×426
	3	7420 (11.5)	W12×120	W14×342	W14×193	W14×500	W14×426
	4	7420 (11.5)	W12×120	W14×342	W14×176	W14×500	W14×426
	5	7420 (11.5)	W12×120	W14×311	W14×159	W14×342	W14×426
	6	7420 (11.5)	W12×120	W14×311	W14×159	W14×342	W14×257
	7	7420 (11.5)	W12×120	W14×159	W14×145	W14×159	W14×257
	8	7420 (11.5)	W12×120	W14×159	W14×132	W14×159	—

Table 5: GMMS design variables

Building	**Equivalent SDOF Stiffness, K_{eq} [10^6 kN m/rad (10^6 kip in/rad)]**	**Roof Drift Ratio at MCE, θ_{MCE} (%)**	λ	N
GMMS-2	1.35 (12.0)	2.40	1.14	2
GMMS-4	3.84 (34.0)	1.95	1.08	4
GMMS-8	8.78 (77.7)	1.78	0.948	4

Table 6: Member sizes for frames determined using the GMMS procedure.

Building	Story	BRB Size [mm^2 (in.^{2})]	Beam	Left Column	Strongback Brace	Strongback Column	Tie Brace
GMMS-2	1	4840 (7.5)	W12×96	W12×72	W12×170	W12×72	—
	2	4840 (7.5)	W12×96	W12×72	W12×72	W12×72	—
GMMS-4	1	6130 (9.5)	W12×96	W12×230	W12×305	W12×279	—
	2	6130 (9.5)	W12×96	W12×230	W12×152	W12×279	W12×210
	3	6130 (9.5)	W12×96	W12×79	W12×152	W12×136	W12×210
	4	6130 (9.5)	W12×96	W12×79	W12×152	W12×136	—
GMMS-8	1	7420 (11.5)	W12×120	W14×550	W14×426	W14×665	—
	2	7420 (11.5)	W12×120	W14×550	W14×342	W14×665	W14×426
	3	7420 (11.5)	W12×120	W14×398	W14×257	W14×550	W14×426
	4	7420 (11.5)	W12×120	W14×398	W14×193	W14×550	W14×426
	5	7420 (11.5)	W12×120	W14×311	W14×193	W14×398	W14×426
	6	7420 (11.5)	W12×120	W14×311	W14×176	W14×398	W14×283
	7	7420 (11.5)	W12×120	W14×159	W14×159	W14×159	W14×283
	8	7420 (11.5)	W12×120	W14×159	W14×159	W14×159	—

Table 7: Member sizes for frames determined using the RSAC procedure.

Building	**Story**	**BRB Size [mm^2 (in.^{2})]**	**Beam**	**Left Column**	**Strongback Brace**	**Strongback Column**	**Tie Brace**
RSAC-2	1	4840 (7.5)	W12×96	W12×72	W12×106	W12×45	—
	2	4840 (7.5)	W12×96	W12×72	W12×50	W12×45	—
RSAC-4	1	6130 (9.5)	W12×96	W12×190	W12×190	W12×106	—
	2	6130 (9.5)	W12×96	W12×190	W12×53	W12×106	W12×58
	3	6130 (9.5)	W12×96	W12×72	W12×72	W12×45	W12×53
	4	6130 (9.5)	W12×96	W12×72	W12×53	W12×45	—
RSAC-8	1	7420 (11.5)	W12×120	W14×398	W14×342	W14×283	—
	2	7420 (11.5)	W12×120	W14×398	W14×159	W14×283	W14×233
	3	7420 (11.5)	W12×120	W14×283	W14×159	W14×159	W14×233
	4	7420 (11.5)	W12×120	W14×283	W14×159	W14×159	W14×159
	5	7420 (11.5)	W12×120	W14×211	W14×159	W14×145	W14×159
	6	7420 (11.5)	W12×120	W14×211	W14×159	W14×145	W14×82
	7	7420 (11.5)	W12×120	W14×159	W14×159	W14×82	W14×82
	8	7420 (11.5)	W12×120	W14×159	W14×159	W14×82	—

Table 8: Weight of strongback braced frame

Building	**Member Weight [kN]**	**Member Weight : RSAC Weight**
SMPA-2	57.0	1.01
SMPA-4	177	1.18
SMPA-8	798	1.47
GMMS-2	66.5	1.18
GMMS-4	232	1.55
GMMS-8	863	1.59
RSAC-2	56.5	1.0
RSAC-4	149	1.0
RSAC-8	542	1.0

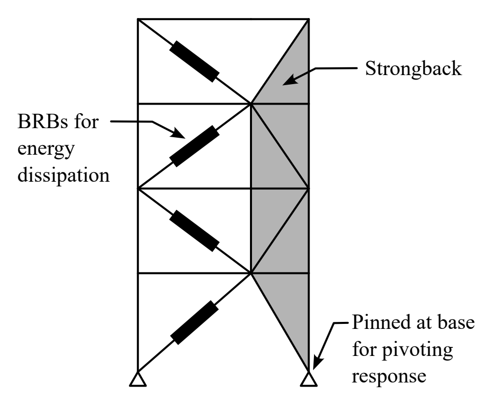
Strongback
BRBs for energy dissipation
Pinned at base for pivoting response

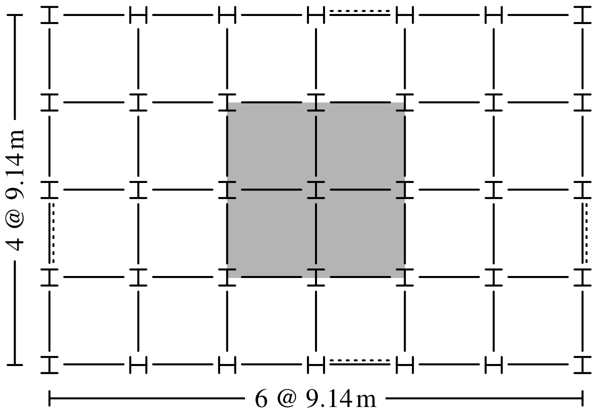
4 @ 9.14m
6 @ 9.14m

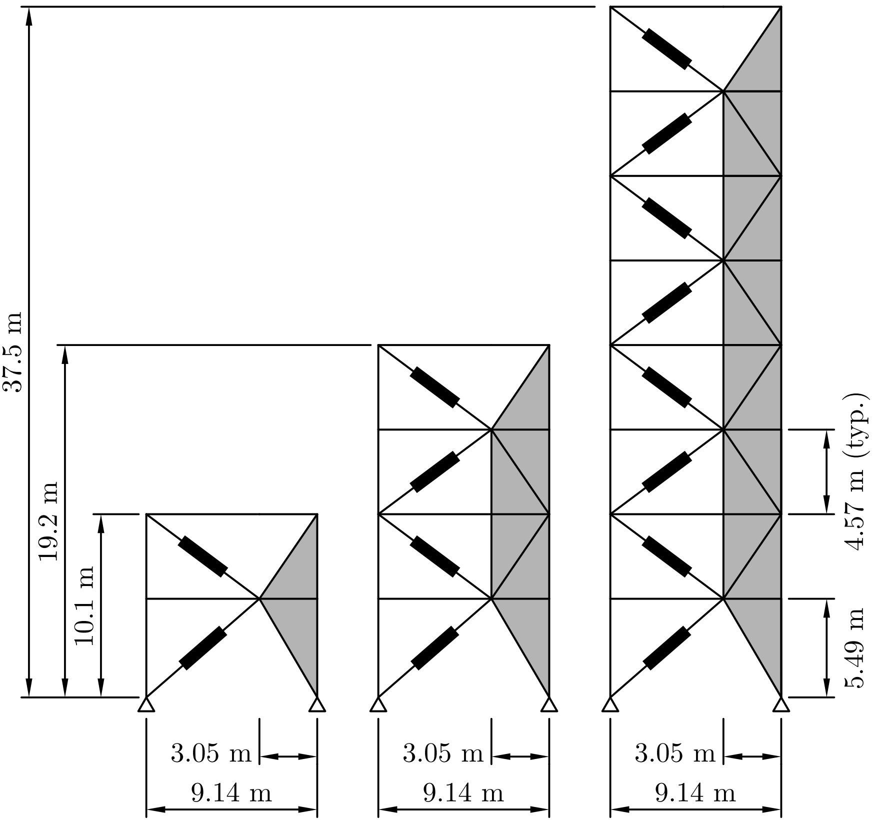

37.5 m
19.2 m
10.1 m
4.57 m (typ.)
5.49 m
3.05 m
9.14 m
3.05 m
9.14 m
3.05 m
9.14 m

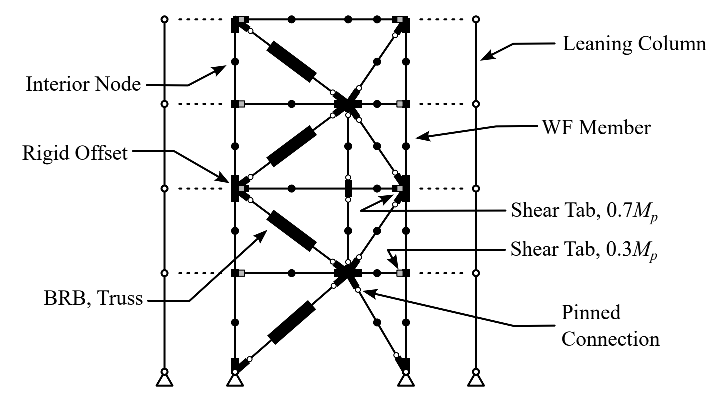
Leaning Column
Interior Node
WF Member
Rigid Offset
Shear Tab, $0.7M_p$
Shear Tab, $0.3M_p$
BRB, Truss
Pinned
Connection

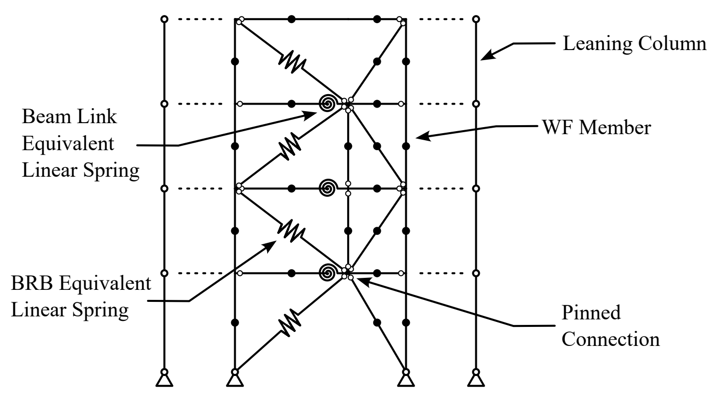
Leaning Column
Beam Link
Equivalent
Linear Spring
WF Member
BRB Equivalent
Linear Spring
Pinned
Connection

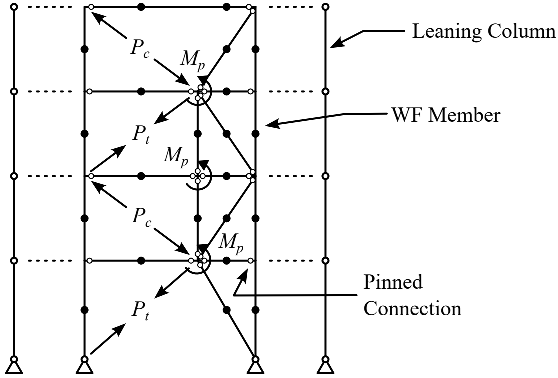

Leaning Column
WF Member
Pinned
Connection
P_c
M_p
P_t
M_p
P_c
M_p
P_t

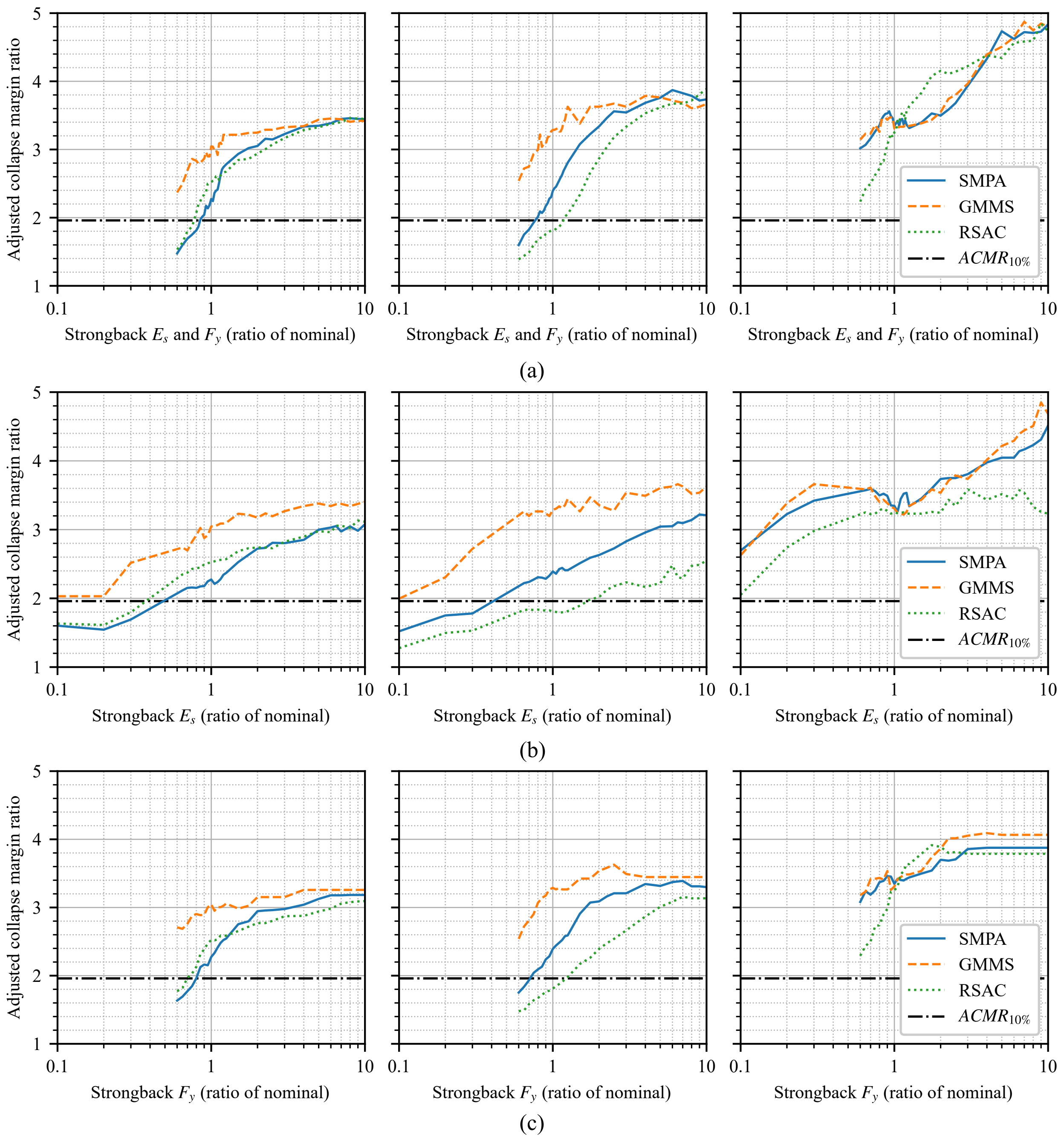

Adjusted collapse margin ratio
Strongback E_s and F_y (ratio of nominal)
(a)
Strongback E_s (ratio of nominal)
(b)
Strongback F_y (ratio of nominal)
(c)
SMPA
GMMS
RSAC
$ACMR_{10\%}$

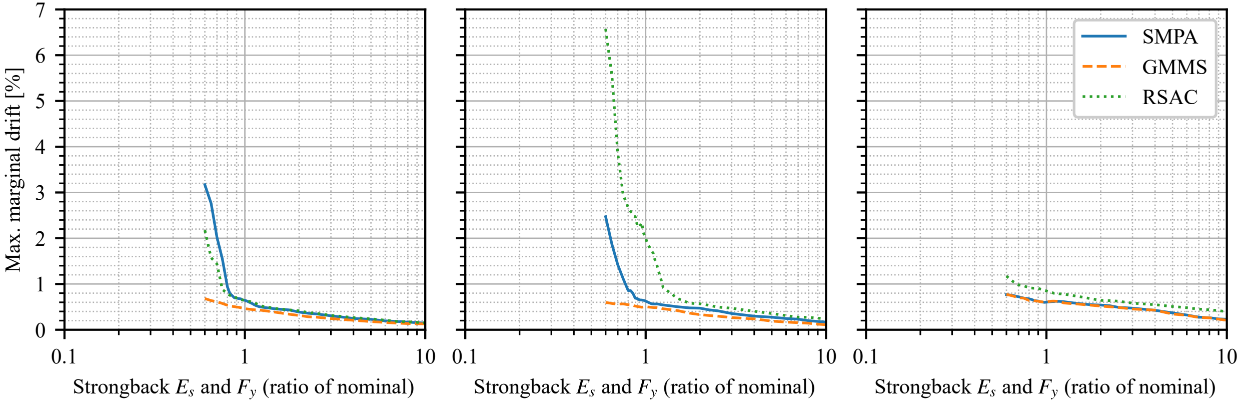

Max. marginal drift [%]
Strongback E_s and F_y (ratio of nominal)
SMPA
GMMS
RSAC

(a)

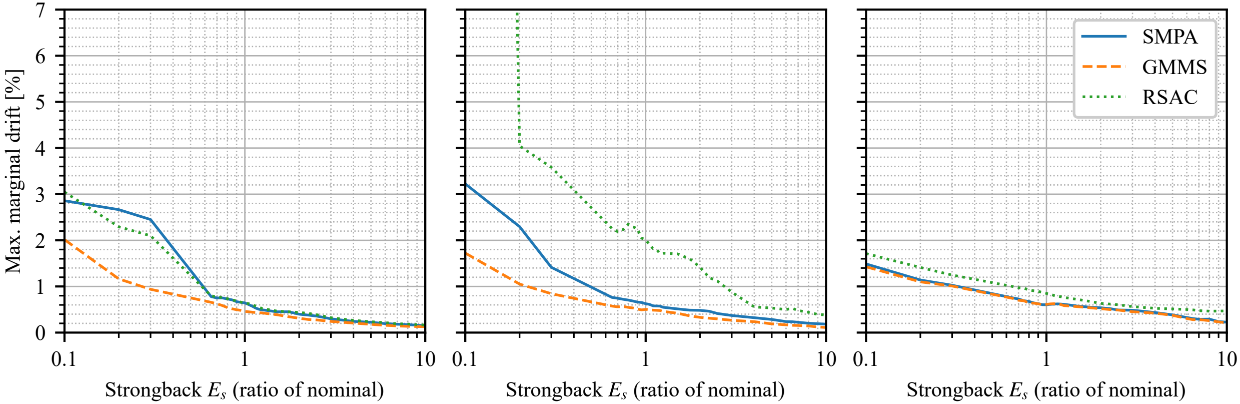

Max. marginal drift [%]
Strongback E_s (ratio of nominal)
SMPA
GMMS
RSAC

(b)

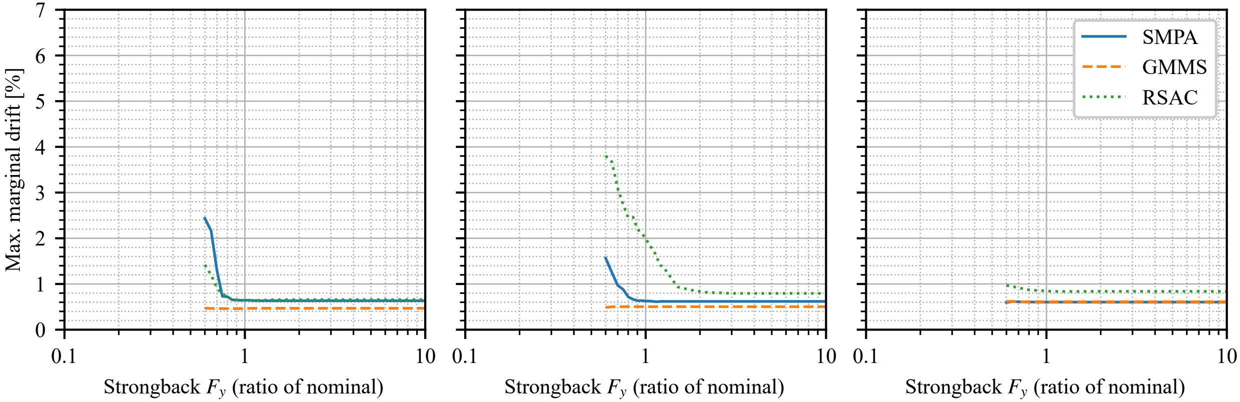

Max. marginal drift [%]
Strongback F_y (ratio of nominal)
SMPA
GMMS
RSAC

(c)

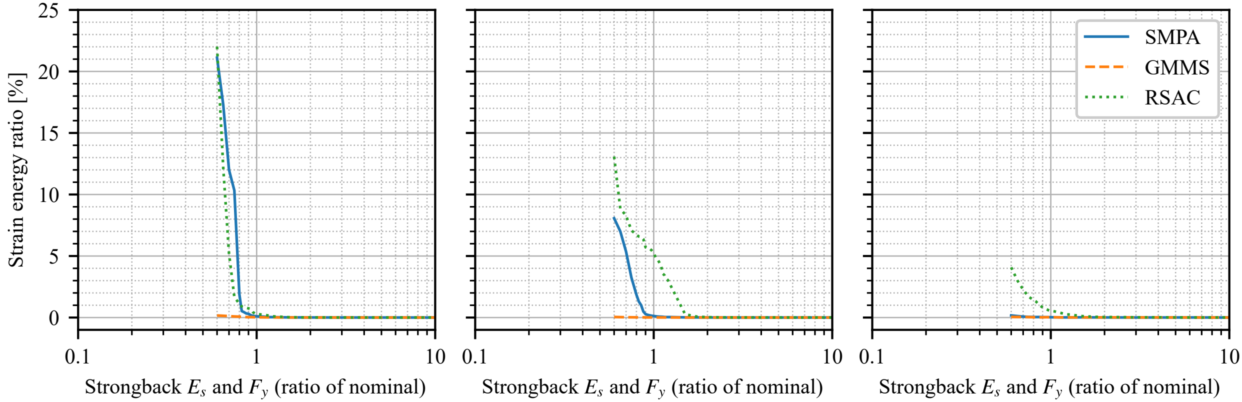
Strain energy ratio [%]
Strongback E_s and F_y (ratio of nominal)
Strongback E_s and F_y (ratio of nominal)
Strongback E_s and F_y (ratio of nominal)
SMPA
GMMS
RSAC

(a)

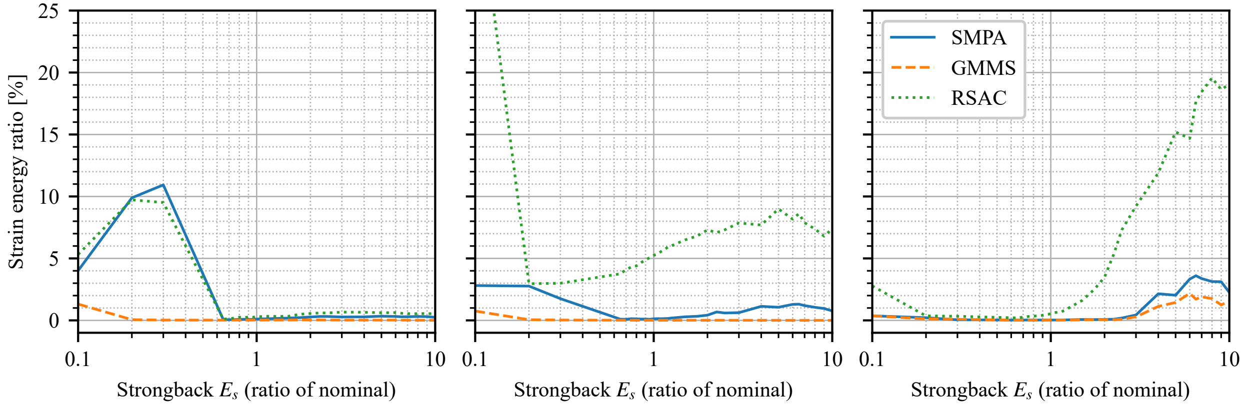
Strain energy ratio [%]
Strongback E_s (ratio of nominal)
Strongback E_s (ratio of nominal)
Strongback E_s (ratio of nominal)
SMPA
GMMS
RSAC

(b)

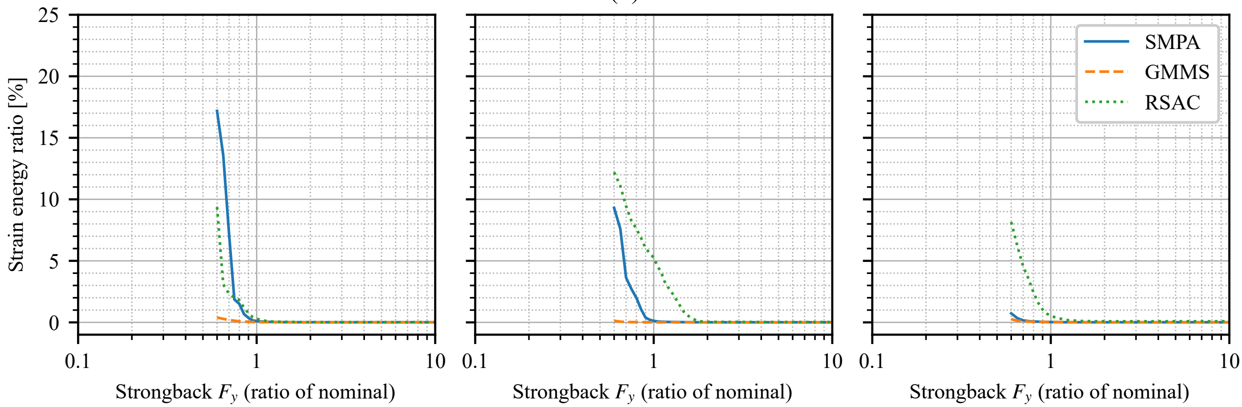
Strain energy ratio [%]
Strongback F_y (ratio of nominal)
Strongback F_y (ratio of nominal)
Strongback F_y (ratio of nominal)
SMPA
GMMS
RSAC

(c)

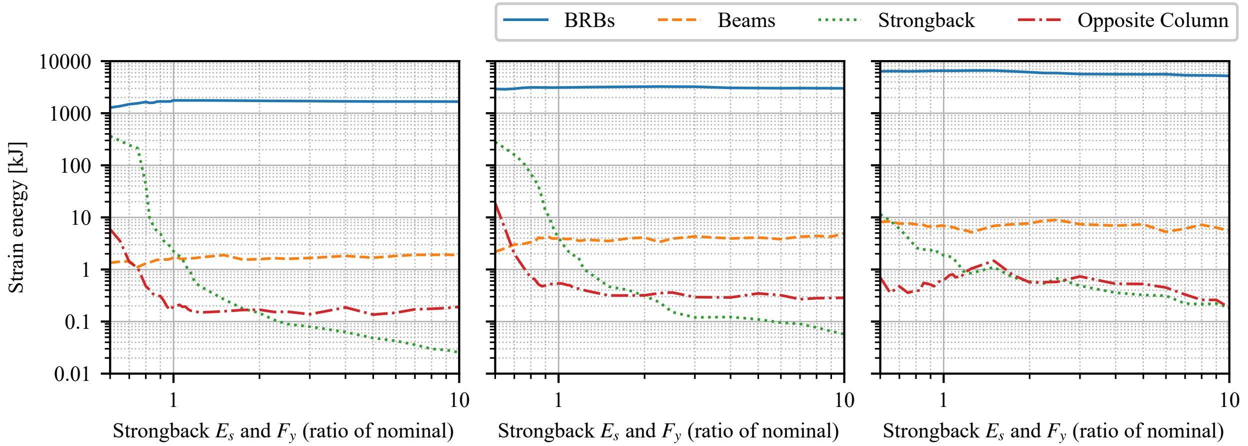
BRBs
Beams
Strongback
Opposite Column
Strain energy [kJ]
10000
1000
100
10
1
0.1
0.01
1
10
Strongback E_s and F_y (ratio of nominal)
1
10
Strongback E_s and F_y (ratio of nominal)
1
10
Strongback E_s and F_y (ratio of nominal)

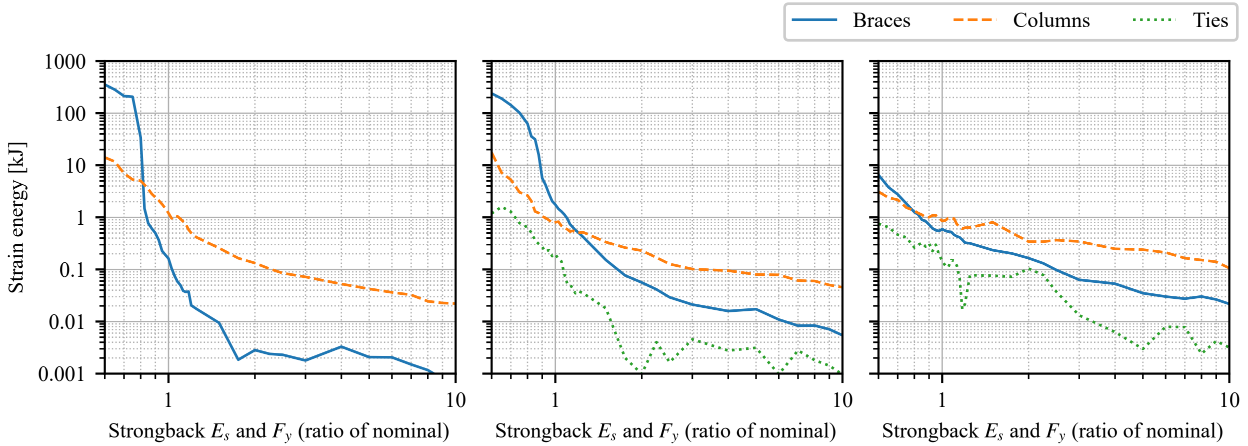

Braces
Columns
Ties
Strain energy [kJ]
1000
100
10
1
0.1
0.01
0.001
1
10
Strongback E_s and F_y (ratio of nominal)
Strongback E_s and F_y (ratio of nominal)
Strongback E_s and F_y (ratio of nominal)

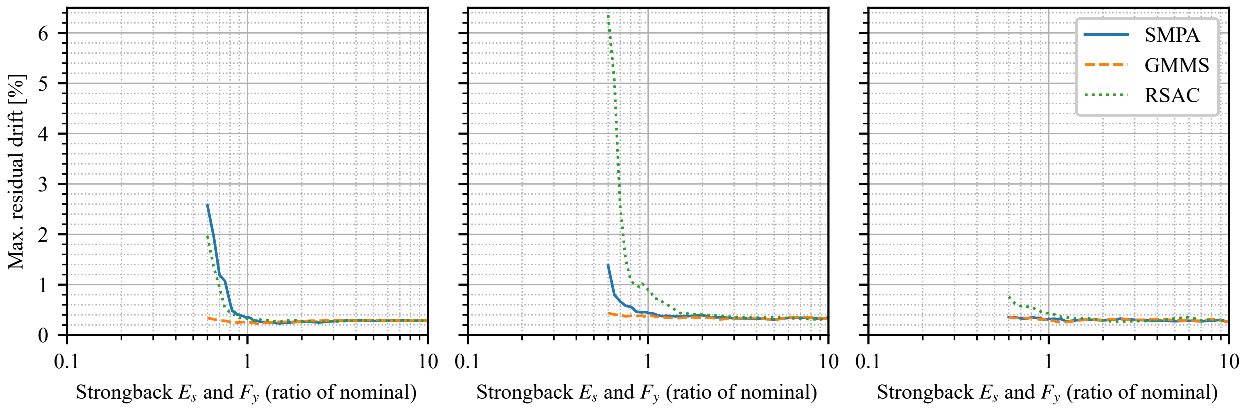

Max. residual drift [%]
0
1
2
3
4
5
6
0.1
1
10
Strongback E_s and F_y (ratio of nominal)
SMPA
GMMS
RSAC